CI&CEQ
Chemical Industry & Chemical Engineering Quarterly

Available online at
Association of the Chemical Engineers of Serbia AChE
www.ache.org.rs/CICEQ

Chem. Ind. Chem. Eng. Q. 30 (2) 161–177 (2024) CI&CEQ

RICARDO ARBACH FERNANDES DE OLIVEIRA
JULIO HENRIQUE ZANATA
GABRIELA CANTARELLI LOPES

Department of Chemical Engineering, Federal University of São Carlos, São Carlos - São Paulo – Brazil

NUMERICAL STUDY OF TURBULENCE ON DRAG COEFFICIENT DETERMINATION FOR PARTICLE AGGLOMERATES

Article Highlights

- A numerical study of the flow around particle agglomerates was performed
- Steady RANS turbulence models were tested to estimate the drag coefficient
- SST k-ω and Spalart-Allmaras turbulence models better represented the flow
- SST k-ω turbulence model presented lower deviations from the empirical correlation
- RNG k-ε presented the worst results, mainly for intermediate Reynolds number

Abstract

Numerical simulations of the flow surrounding particle agglomerates were carried out using computational fluid dynamics to assess the ability of five RANS turbulence models to estimate the drag coefficient in particle agglomerates. Simulations were carried out in steady conditions for Reynolds numbers between 1 and 1500. Streamlines showed that symmetrical agglomerates present a velocity profile similar to the single sphere profile. Results showed that both Spalart-Allmaras and SST k-ω turbulence models could represent the flow profile in the regions near and far from the walls of the agglomerates and the wake region in the rear of the agglomerates. The RNG k-ε model showed poor quality in predicting the velocity profile and the drag coefficient. The drag coefficient obtained by simulations presented a trend better represented by the Tran-Cong model, also showing that deviations from the predictions decreased as the packing density of the agglomerate increased. The use of steady RANS simulations showed to be a feasible and efficient method to predict, with low computational cost, the drag coefficient in particle agglomerates. For the transition and turbulent flows, results presented good agreement, with deviations between -15% and 13%, while for lower Reynolds numbers, deviations varied between -25% and 5%.

Keywords: particulate matter, particle agglomerates, turbulence, drag coefficient, computational fluid dynamics.

SCIENTIFIC PAPER

UDC 532.5:519

In designing equipment involving particle-laden flows, it is essential to correctly model the interaction between the two phases to obtain consistent results. The forces of fluid-particle interaction are directly related to the characteristics of the particles, such as size, shape, elasticity, and roughness, which are determinants in the performance of equipment such as the fluidized bed [1–4]. Usually, in models that simulate fluidized bed reactors, the drag force is related to the porosity of the bed, assuming that the particles are distributed homogeneously [5–8]. However, depending on their physical, superficial, and mechanical characteristics, the collision, attraction, and friction between the particles can lead to the formation and irregular distribution of agglomerates, altering the flow dynamics through pressure oscillations [9,10].

Indeed, the behavior of particle agglomeration in different arrangements deserves attention, as it occurs in almost all forms, whether naturally or artificially. One can find such kind of irregularly shaped particles in

Correspondence: G.C. Lopes, Department of Chemical Engineering, Federal University of São Carlos, Rodovia Washington Luís, km 235 - SP-310, São Carlos - São Paulo - Brazil, P.O. Box: 13565-905.
E-mail: gclopes@ufscar.br
Paper received: 6 December, 2022
Paper revised: 4 June, 2023
Paper accepted: 14 August, 2023

https://doi.org/10.2298/CICEQ221206021O

many applications, such as sedimentation and flocculation of fine particle aggregates in rivers and lakes, chemical mixing, mineral processing, stirred tanks, powder sintering, and manufacturing with phase change processes [11–13]. For several of these processes, determining the particle's terminal velocity is an important stage for designing and optimizing processes and equipment. Since this velocity is straightly dependent on the body's drag coefficient, such a study is important to simulate the movement of such particles.

Due to the lack of an analytical solution, the literature presents several empirical correlations designed to predict the drag coefficient of spherical and non-spherical particles associated with different ranges of validity and precision [14–19]. To obtain predictions that better represent the empirical observations, shape descriptors have been developed in recent decades to quantify aspects such as shape, circularity, roughness, and sphericity. However, the correlations present some disadvantages, such as the fact that the first studies are mainly, based on experiments with regularly-shaped particles such as cubes, cylinders, and disks, which reduces the level of detail and accuracy in the description of the local scale phenomena [20,21].

For the evaluation of the drag coefficient of isolated groups of ordered packed spheres moving through Newtonian fluids, Tran-Cong *et al.* [11] conducted laboratory measurements, leading to a correlation with good agreement over a limited range of Reynolds numbers and body dimensions but covering most of the irregularly shaped particles in engineering applications. Beetstra *et al.* [20] compared these experimental data with lattice-Boltzmann simulations for the same conditions, aiming to expand the field of the influence of the geometry on the disturbance of fluidized beds, stating that, indeed, the drag force on each particle is strongly dependent on the inter-particle distance variation. The results showed how the omission of the agglomeration effect could cause deviations between the simulated equipment behavior and experimental results.

The literature presents studies using the lattice-Boltzmann method (LBM) and Direct Numerical Simulation (DNS) to evaluate particle drag coefficients. For industrial-scale problems, these approaches are considered impractical, due to the high computational effort, mainly for high Reynolds numbers, since the simulations must be carried out in a transient formulation with small timesteps and the mesh must be fine enough, to respect the Kolmogorov scales [22,23]. However, in the field of sub-grid scale, they are very useful for understanding the influence of turbulence in small-scale vortices. The LBM is useful for CFD to understand particle flow due to the algorithm's simplicity and explicit methods [24]. Since the method presents a high resolution of the domain, the studies present better accuracy, as observed in studies such as Dietzel and Sommerfeld [25], that used the LBM to investigate complex geometry with a high discretization around the agglomerate and obtained deviations lower than 10% for lower values of Reynolds, where deviations are generally by the order of 20% [25].

DNS is an important tool to estimate, with accuracy, correlations for the micro-scale transport coefficients, one of the essential parameters for coarse-grained models of fluid-particle systems [21]. To understand the fluid-particle mass transfer in random arrays of particles, Mehrabadi *et al.* [26] performed DNS in a homogeneous flow, aiming to isolate the effect of interphase interactions on a particle agglomerate, developing a gas-solid drag law for clustered particles based on the conclusion that particle clusters lead to a drag reduction. Another recent example of this method is the study of Chen *et al.* [27], where the drag and lift in particle agglomerates were studied for different orientations and sizes of particles and presented deviations between 2 and 4%. However, due to the method's constraints, the study focused on understanding the hydrodynamic on agglomerates for a range of Reynolds below 100, highly dependent on the projected area [25].

In contrast to the large number of empirical correlations to predict the drag coefficient of irregular particles, there is a scarcity of studies in which specific correlations have been proposed to determine drag forces acting on particle agglomerates. The literature in the computational field using the unsteady formulation, such as LES and DNS, focuses on analyzing simple bodies – such as regularly-shaped single bodies – due to the difficulty in generating uniform meshes around complex bodies, as well as limited to low Reynolds flows, generally below 250, due to the computational demands associated with higher Reynolds numbers [22]. The use of LBM eliminates the difficulty of mesh generation, so we observe studies on more complex and arbitrary bodies [25] with an agglomeration of several spheres. However, the method is still limited for low Reynolds flows since the forces acting on walls inside the flow are directly calculated in the smaller scales [20,21,24–27].

Because of the lack of studies for higher Reynolds flows and since the high computational cost needed to perform transient simulations, we focus on proposing a methodology using the steady formulation to simplify the problem of calculating the drag coefficient in complex bodies, which allowed the investigation of the flow for a wide range of Reynolds numbers. Since

turbulence plays an important role in the flow profile as we increase the velocity of the fluid, we focused on how its modeling interferes with the drag estimation in particle agglomerates. So, the present paper evaluates the drag coefficient of three different conformations of irregularly shaped particle agglomerates composed of spherical particles surrounded by a water flow, varying the turbulence model tested. The models were compared using steady RANS turbulence models to investigate their robustness to predict the drag acting in particle agglomerates for different conformations to reduce the computational costs of unsteady simulations, such as URANS, LES, DNS, or LBM.

MATERIALS AND METHODS

Materials

This study was carried out in the theoretical field, using CFD simulations to obtain the flow profile of water around particle agglomerates. The drag coefficient of the particles was calculated by CFD simulations using five different turbulence models. The results were compared with five empirical correlations for estimating the drag coefficient in irregularly-shaped particles present in literature to find which is robust enough to represent the trend of the results of the drag coefficient in particle agglomerates obtained by simulations.

In the theoretical field, the drag coefficient for spheres is simple to calculate since it depends on a balance of forces. This balance leads to Eq. (1)

$$C_p = \frac{F_D}{0.5\rho_f A\left|u_p - u_f\right|\left(u_p - u_f\right)} \tag{1}$$

where F_D is the drag force. The drag depends on the fluid, particle, and flow characteristics, i.e., fluid density and velocity, ρ_f and u_f, respectively, and the particle velocity and reference area, u_p and A, respectively. The particle in the domain of the present study is fixed, leading to a particle velocity equal to zero, so the fluid flow profile and the drag coefficient are given exclusively by the behavior of the fluid flow around the particle.

To determine which correlation better follows the trend observed in the drag coefficient obtained by CFD, we must define some criteria to compare the simulations with the correlations. The first consideration was analyzing and comparing the flow profile for each of the five turbulence models with the behavior expected by the literature. This step is important to understand if the results obtained for the drag coefficient are reliable.

Since a quantitative analysis is crucial, we also evaluated the percent deviation between simulations and correlations, estimated by Eq. (2).

$$\sigma = 100\frac{C_D^{corr} - C_D^{sim}}{C_D^{corr}} \tag{2}$$

where C_D^{corr} and C_D^{sim} are the drag coefficients obtained by the correlation and the simulation, respectively. Another quantitative analysis considered was the root-mean-square error, *RMSE*, given by

$$RMSE = \sqrt{\frac{\sum_{i=1}^{N}\left(\hat{x}_i - x_i\right)^2}{N}} \tag{3}$$

where $\hat{x}_i$ is the value of the i^{th} data of a parameter estimated by the correlation, x_i is the value of the i^{th} data of the parameter obtained by simulation – i.e., the drag coefficient – and N is the local data in the sample studied.

Numerical simulations

The numerical simulations were carried out using the software ANSYS 14.5. The computational domain and numerical meshes of the particle agglomerates in this study were generated using the software ANSYS Design Modeler and Meshing. ANSYS Fluent 14.5 was used to solve the model equations. CFD-Post was used to analyze the fluid flow profile and the drag coefficient.

Design and mesh generation

Simulations were carried out for three different computational domains, varying the geometry of the agglomerates containing three, four, and five particles, where the radius of each particle in the agglomerate measures 0.5 cm. The domain generated corresponds to a parallelepiped with a height and width of 0.1 m and a length of 0.2 m.

Aiming to generate well-structured meshes, the domain was divided into two cubes, as presented in Figure 1. The cube on the left side, close to the inlet, was subdivided into seven smaller parts to control better the quality of the elements around the agglomerate of spheres. Six of them are pyramidal-shaped, connected to an inner cube, surrounding the agglomerate of spheres, and positioned in the center of the major cube. For the second cube, on the right side and close to the outlet, it was unnecessary to divide it into smaller parts. Figure 1 also shows a cut of the lateral view of the computational domain using the agglomerate of five spheres as an example, while Figure 2 shows the isometric view of the geometry of the three agglomerates.

Meshes statistics

Before running simulations, it is important to

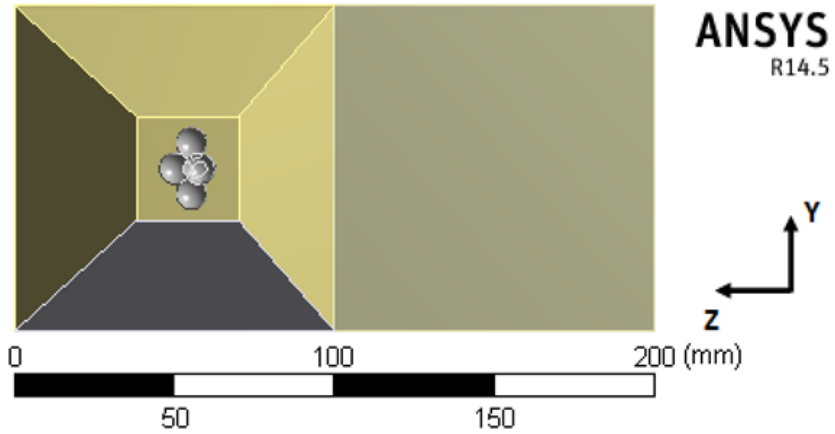

Figure 1. Example of the lateral view of the interior of the computational domains simulated.

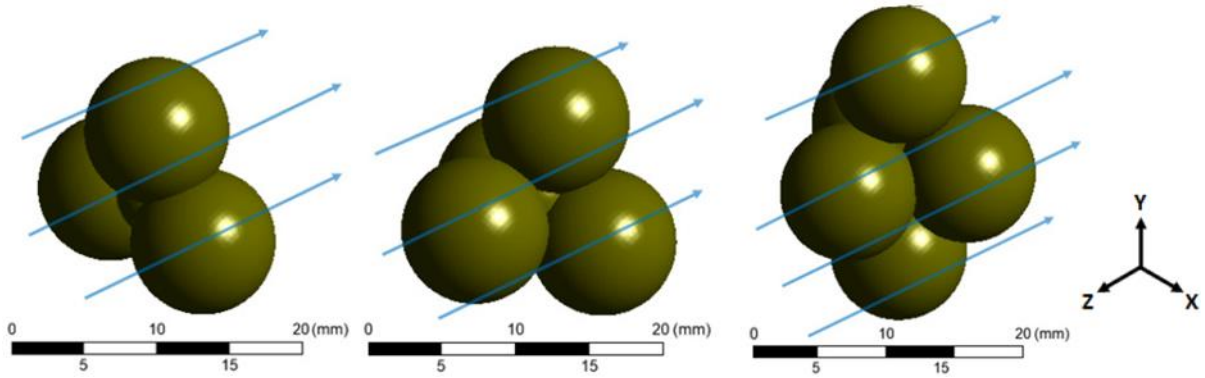

Figure 2. From left to right: Isometric view of the particle agglomeration of three, four, and five particles and a scheme of the flow direction.

analyze the quality of the mesh by verifying the elements according to their shape and criteria for several mesh quality parameters. In this study, its aspect ratio, orthogonality, and skewness were evaluated. To obtain convergence stability easier and better accuracy, it is ideal to have elements exclusively hexahedral. However, hybrid meshes were generated due to the complexity of the agglomerates' geometry. These meshes contain elements with shapes referred to as tetrahedral, six-node wedge, five-node pyramid, and hexahedral.

To avoid distorting the mean values and standard deviations, the values are presented separately according to two regions: the inner cube around the agglomerate (Figure 1), referred to as the subdomain, and the whole computational domain, referred to as the total domain. Table 1 shows the values of the minimum, maximum, mean, and standard deviation of the three parameters for the tested meshes, detailed for the subdomain and the total domain.

The minimum value possible for the aspect ratio is 1, where the quality is considered excellent for values lower than 20 [28,29]. For both the total domain and subdomain, the maximum values obtained were above 20. However, their average values are lower than 1.2, with standard deviations lower than 0.48%. Analyzing the aspect ratio of the three meshes presented in Table 2, we find many elements with values below 5, which are considered excellent for this criterion.

The orthogonality varies from 0 to 1, where values above 0.8 are considered excellent [28,29]. Even though some elements present poor quality, the mean value for each proposed domain was above 0.94, with a standard deviation lower than 0.1%, where elements with orthogonality above 0.8 correspond to at least 94% of the elements, as seen in Table 2. It occurs due to the high quantity of hexahedrons, which tend to have higher orthogonality. This effect is also present in skewness. Analyzing the skewness, where elements have excellent quality for values between 0 to 0.2 and good quality for values between 0.2 and 0.4, we observe that the mean values do not exceed 0.07, and the standard deviations do not exceed 0.12% for any mesh. The low value directly results from the high quantity of hexahedrons with good and excellent quality.

Pyramidal shapes, such as tetrahedrons and five-

Table 1. Mesh quality for the three agglomerates studied.

Mesh quality parameter		Subdomain			Total domain		
		3 spheres	4 spheres	5 spheres	3 spheres	4 spheres	5 spheres
Aspect ratio	Minimum	1	1	1	1	1	1
	Maximum	32.12	24.58	299.98	32.12	24.58	299.98
	Mean	1.123	1.186	1.187	1.061	1.069	1.076
	SD (%)	0.403	0.476	0.547	0.284	0.306	0.349
Orthogonality	Minimum	0.212	0.152	0.032	0.210	0.152	0.032
	Maximum	1	1	1	1	1	1
	Mean	0.962	0.944	0.944	0.987	0.984	0.982
	SD (%)	0.081	0.093	0.095	0.052	0.056	0.060
Skewness	Minimum	0	0	0	0	0	0
	Maximum	0.975	0.993	0.987	0.982	0.997	0.999
	Mean	0.041	0.062	0.063	0.018	0.022	0.024
	SD (%)	0.120	0.142	0.114	0.078	0.088	0.094

Table 2. Percentage of elements of the meshes attending to the criteria of the quality coefficients.

Region	Agglomerate	Number of elements	Aspect ratio Below 5 (%)	Orthogonality Above 0.8 (%)	Skewness Below 0.4 (%)
Subdomain	3 spheres	1240970	99.99	96.24	96.39
	4 spheres	1064255	99.96	94.25	94.59
	5 spheres	1328015	99.97	94.21	94.41
Total domain	3 spheres	5234907	99.99	98.67	98.64
	4 spheres	5001753	99.99	97.89	98.17
	5 spheres	5220320	99.98	97.98	97.87

node pyramids, are expected to have lower orthogonality and higher skewness [29]. Table 2 shows that the influence of such shapes on the quality of the meshes was not significant because of the low number of pyramidal elements – representing less than 2.5% of the elements of the subdomain and less than 0.5% of the total domain for all meshes.

It is relevant to emphasize the predominance of hexahedral elements for both subdomain and total domain in all meshes. The agglomerate of three spheres presented percentages of hexahedral elements above 83% in the subdomain and 93% in the total domain. In the meshes of agglomerates of four and five spheres, these percentages were above 92% in the subdomain and 95% in the total domain. Also, analyzing the meshes statistics for three main parameters, the elements have good or excellent quality, so the meshes are expected to behave with convergence stability and obtain accurate results.

The governing equations

The time-averaged conservation equations for the steady incompressible isothermal turbulent flow in the three-dimensional model, neglecting body force, can be expressed by the equations of continuity and motion [22].

The closure equations for the RANS approach depend on the turbulence model used. In this study, we investigated the effects of five turbulence models. The models are classified according to the number of transport equations used to close the modeling of the problem. The tested models are the one-equation-based Spalart-Allmaras, the two-equation-based RNG k-ε, SST k-ω, the four-equation-based Langtry-Menter, and the six-equation Reynolds stress model. The modeling of its closure equations and coefficients is better detailed in the literature [30–34].

Simulation setup

The fluid properties were set up for an isothermal operation condition of 25 °C, obtaining water density and viscosity of 998.2 kg/m^3 and 1.003 x 10^{-3} Pa·s, respectively. As a boundary condition, the inlet velocity of the water was set as an injection normal to the inlet surface. Since the drag experienced by particles flowing in a Newtonian fluid can be divided into seven main flow regimes according to its Reynolds number, we varied the velocities of the flow to obtain Reynolds numbers between 1 and 1500 to ensure that we will observe how the turbulence model interferes on the

estimation of the drag coefficient in all the regimes, from laminar to turbulent wake flow regimes [35,36]. The velocities varied from 5 x 10^{-5} to 0.10501 m/s, as presented in Table 3, according to the agglomerate, to obtain the range of Reynolds numbers proposed, calculated by Eq. (4).

$$\mathrm{Re} = \frac{\rho\, u\, d_{eq}}{\mu} \tag{4}$$

where ρ, u, μ are the density, relative velocity, and viscosity of the fluid, and d_{eq} is the diameter of the sphere equivalent to the agglomerate, i.e., with the same volume. Unsteady simulations were also carried out at the higher Reynolds number to compare the difference between the drag coefficients. Despite presenting the unsteady turbulent wake profile, the drag coefficient obtained did not present significant deviations, so we chose the steady simulations to reduce computational efforts. The boundary conditions were set to the no-slip condition for the sphere walls and specified shear for the domain walls.

Table 3. Inlet velocity of the flow for the Reynolds numbers tested.

Reynolds	Velocity (m/s)		
(-)	3 spheres	4 spheres	5 spheres
1	0.000070	0.000064	0.000059
5	0.000350	0.000318	0.000295
10	0.000700	0.000636	0.000590
30	0.002100	0.001907	0.001770
50	0.003500	0.003178	0.002950
80	0.005600	0.005085	0.004720
100	0.007000	0.006356	0.005900
300	0.021002	0.019069	0.017702
500	0.035003	0.031781	0.029503
800	0.056005	0.050849	0.047205
1000	0.070007	0.063562	0.059006
1300	0.091009	0.082631	0.076708
1500	0.105010	0.095343	0.088509

Despite the SIMPLE-based algorithms presenting lower computational effort [37], we chose the PISO algorithm since it presents greater stability, requiring fewer iterations, generating a faster convergence, and, consequently, less processing time [38,39].

The spatial discretization was set to the least-squares cell-based method for gradients, *PRESTO*! scheme for pressure and second-order upwind scheme for energy, momentum, and turbulence equations to solve the problem of underestimation of turbulent kinetic energy and its dissipation rate, as suggested in previous studies [12,13].

Turbulence closure models

The choice of the turbulence models was based on their characteristics and ability to solve specific problems presented by the complex geometry of the meshes generated. Since one of the focuses in the present study stands on analyzing the drag coefficient in an agglomerate of particles, predicting the flow in the boundary layer is essential. The Spalart-Allmaras model, a one-equation-based model, fits in this type of flow since it was developed to study the flow in the boundary layers of airfoils [28]. Two other models also developed to represent this zone are the transition models SST k-ω and the Langtry-Menter k-ω [22]. The first one is a two-equation-based model that solves the equation of the turbulent kinetic energy, k, for the flow far from the wall and, for the boundary layer, weights the influence of the turbulent kinetic turbulence and the specific turbulence dissipation rate, ω, using blending functions. The second is based on the k-ω. However, it implements two transport equations, one to solve the intermittency, γ, and one to solve the transition momentum-thickness Reynolds number, $\widetilde{Re}_{\theta t}$, to better represent profiles with strong adverse pressure gradients [32,33,40].

We also tested turbulence models developed to represent wide ranges of Reynolds numbers. With a low computational cost, the k-ε model was developed to solve several engineering in a wide range of Reynolds numbers [41]. This model has the characteristic of modeling the near-wall region and solving the transport equation for the outer region of the boundary layer. We chose to use the RNG k-ε, an improvement of the k-ε developed to solve problems where the flow presents a highly swirling profile [31]. The Reynolds stress model was another model tested in this study, with similar characteristics but more robust. The main difference in this seven-equation-based model that leads to its robustness is the addition of six transport equations, one for each independent Reynolds stress, to the solution for the dissipation equation, ε, and its anisotropic treatment [34]. The following items are reserved for modeling the transport equations of each turbulence model presented.

i. Spalart-Allmaras Model

The Spalart-Allmaras is a one-equation model that solves a viscosity-like variable's transport equation. $\tilde{\nu}$, also referred to as the Sparlat-Allmaras variable. The model is given by Eq. (5):

$$\frac{\partial \bar{\nu}}{\partial t} + \frac{\partial\left(u_j \bar{\nu}\right)}{\partial x_j} = \frac{1}{\sigma}\frac{\partial}{\partial x_j}\left[\left(\nu + \bar{\nu}\right)\frac{\partial \bar{\nu}}{\partial x_j}\right] + \frac{c_{b2}}{\sigma}\frac{\partial \bar{\nu}}{\partial x_j}\frac{\partial \bar{\nu}}{\partial x_j} + c_{b1}\bar{S}\bar{\nu} - c_{\omega 1} f_{\omega}\left(\frac{\bar{\nu}}{d}\right)^2 \tag{5}$$

where $\tilde{S}$ is the production of turbulent viscosity, c_{b1}, c_{b2}, c_{w1}, f_w, and σ are the model's closure coefficients and auxiliary relations, better described by Spalart and Allmaras [30].

ii. RNG k-ε Model

The RNG k-ε model uses the renormalization group theory to improve the Standard k-ε model, which models the turbulence kinetic energy, k, and the turbulence dissipation rate, ε, given by Eqs. (6) and (7), respectively,

$$\frac{\partial k}{\partial t}+\frac{\partial\left(u_i k\right)}{\partial x_i}=\frac{\partial}{\partial x_j}\left[\left(\nu+\frac{\nu_t}{\sigma_k}\right)\frac{\partial k}{\partial x_j}\right]+P_k-\varepsilon \tag{6}$$

$$\frac{\partial \varepsilon}{\partial t}+\frac{\partial\left(u_i \varepsilon\right)}{\partial x_i}=\frac{\partial}{\partial x_j}\left[\left(\nu+\frac{\nu_t}{\sigma_\varepsilon}\right)\frac{\partial \varepsilon}{\partial x_j}\right]+C_{1\varepsilon}\frac{\varepsilon}{k}P_k-C_{2\varepsilon}^{*}\frac{\varepsilon^2}{k} \tag{7}$$

where P_k is the production term of the turbulent kinetic energy [31].

iii. SST k-ω Model

The SST k-ω model modifies low-Reynolds number effects, compressibility, and shear flow spreading. The model is based on modeling transport equations for turbulence kinetic energy and the specific dissipation rate, given by Eqs. (8) and (9), respectively.

$$\frac{\partial k}{\partial t}+\frac{\partial\left(u_i k\right)}{\partial x_i}=\frac{\partial}{\partial x_j}\left[\left(\nu+\sigma_k \nu_t\right)\frac{\partial k}{\partial x_j}\right]+P_k-\beta^{*}k\omega \tag{8}$$

$$\frac{\partial \omega}{\partial t}+\frac{\partial\left(u_i \omega\right)}{\partial x_i}=\frac{\partial}{\partial x_j}\left[\left(\nu+\sigma_\omega \nu_t\right)\frac{\partial \omega}{\partial x_j}\right]+ 2\left(1-F_1\right)\sigma_{\omega 2}\frac{1}{\omega}\frac{\partial k}{\partial x_i}\frac{\partial \omega}{\partial x_i}+\alpha\mathcal{S}^2-\beta\omega^2 \tag{9}$$

where F_1 is the blending function, α, β, and σ refer to the closure coefficients of the model [32].

iv. Langtry-Menter SST k-ω Model

Modeled similarly to the SST k-ω model presented previously, the Langtry-Menter model implements two transport equations to solve the intermittency and the turbulent transition Reynolds number, given by Eqs. (10) and (11), respectively.

$$\frac{\partial \gamma}{\partial t}+\frac{\partial\left(u_i \gamma\right)}{\partial x_j}=\frac{\partial}{\partial x_j}\left[\left(\nu+\frac{\nu_t}{\sigma_f}\right)\frac{\partial \gamma}{\partial x_j}\right]+P_{\gamma 1}-E_{\gamma 1}+P_{\gamma 2}-E_{\gamma 2} \tag{10}$$

$$\frac{\partial \bar{\mathrm{Re}}_{\theta t}}{\partial t}+\frac{\partial\left(u_j \bar{\mathrm{Re}}_{\theta t}\right)}{\partial x_j}=\frac{\partial}{\partial x_j}\left[\sigma_{\theta t}\left(\nu+\nu_t\right)\frac{\partial \bar{\mathrm{Re}}_{\theta t}}{\partial x_j}\right]+P_{\theta t} \tag{11}$$

where $P_{\gamma 1}$ and $E_{\gamma 1}$ are the transition sources, $P_{\gamma 2}$ and $E_{\gamma 2}$ are the destruction sources and $P_{\theta t}$ is a source term [33].

v. Reynolds Stress Model

The RSM consists of modeling the Reynolds stresses, represented by the tensor τ, and the turbulence dissipation rate, ε [22]. The exact transport equation of the Reynolds stresses, in tensorial notation, is given by Eq. (12).

$$\frac{\partial \tau_{ij}}{\partial t}+\bar{u_k}\frac{\partial \tau_{ij}}{\partial x_k}=\frac{\partial}{\partial x_k}\left[\frac{\nu_t}{\sigma_k}\frac{\partial \tau_{ij}}{\partial x_k}\right]+P_{ij}-C_1\frac{\varepsilon}{K}\left[\tau_{ij}-\frac{2}{3}\delta_{ij}K\right]- C_2\left[P_{ij}-\frac{2}{3}\delta_{ij}P\right]-\frac{2}{3}\delta_{ij}\varepsilon \tag{12}$$

where the turbulence production terms P_{ij} are given by

$$P_{ij}=-\left[\tau_{ik}\frac{\partial \bar{u_j}}{\partial x_k}+\tau_{jk}\frac{\partial \bar{u_i}}{\partial x_k}\right] \tag{13}$$

where P is the fluctuation kinetic energy production and ν_t the turbulent kinematic viscosity.

The transport equation for turbulence dissipation rate, ε, is given by

$$\frac{\partial \varepsilon}{\partial t}+\bar{u_j}\frac{\partial \varepsilon}{\partial x_j}=\frac{\partial}{\partial x_j}\left[\left(\nu+\frac{\nu_t}{\sigma_\varepsilon}\right)\frac{\partial \varepsilon}{\partial x_j}\right]-C_{\varepsilon 1}\frac{\varepsilon}{K}\tau_{ij}\frac{\partial \bar{u_i}}{\partial x_j}-C_{\varepsilon 2}\frac{\varepsilon^2}{K} \tag{14}$$

where $K=\frac{1}{2}\overline{u_i' u_i'}$ is the fluctuation of kinetic energy [34].

Drag coefficient correlation modelling

For several applications in industry, the drag force is the main acting force on a particle in the opposite direction of the particle motion.

Studies generally consider the most influential parameters to estimate the drag coefficient, i.e., the particle Reynolds number, shape, orientation, and particle-to-fluid density ratio. Also, secondary parameters, such as secondary motions, turbulence, and particle/fluid acceleration, are the focus of studies [11,16,17,20,42–45].

The present study considered five correlations observed in the literature that consider only the main parameters, as follows. Four of them consider the Reynolds number and shape parameters, such as the sphericity, circularity, and flatness of the agglomerate [11,16,17,19], while one of them uses the orientation of the agglomerate to estimate two different shape parameters [18].

Haider and Levenspiel model

The study of Haider and Levenspiel [16] was the first to propose that the drag coefficient is a function of

the Reynolds number and sphericity for both spherical and nonspherical particles. Also, the Reynolds number should be calculated using an equivalent diameter, d_{eq}, corresponding to the diameter of a sphere with the same volume of the particle tested. They proposed that drag correlations could be written as

$$C_D = \frac{24}{\mathrm{Re}}\left(1 + A\mathrm{Re}^B\right) + \frac{C}{1 + \frac{D}{\mathrm{Re}}} \tag{15}$$

where A, B, C, and D are parameters given as a function of the sphericity Φ and are applicable for $Re < 2.5 \cdot 10^4$ for isometric particles [16], such as the one proposed in the present study.

Ganser model

The model proposed by Ganser [17] adapts the Haider & Levenspiel model, introducing two other shape-dependent parameters: Newton's and Stokes' parameters, k_N and k_S, respectively, and is given by Eq. (16).

$$C_D = \left(24\frac{k_S}{\mathrm{Re}}\right)\left[1 + 0.1118\left(\mathrm{Re}\frac{k_N}{k_S}\right)^{0.6567}\right] + \frac{0.4305 k_N}{1 + \frac{3305}{\mathrm{Re}\,k_N / k_S}} \tag{16}$$

where k_N and k_S are functions of the sphericity, Φ, and the model is applicable for $Re < 3 \cdot 10^5$ if k_N and k_S are known. The literature presents several proposals to estimate these parameters, such as the Tran-Cong et al. [11], Hölzer and Sommerfeld [18], and Bagheri and Bonadonna [19], tested in this study and presented in the following sections.

Tran-Cong *et al.* model

The model proposed by Tran-Cong *et al.* [11] considers that the drag coefficient is a function not only of the Reynolds number but also of the ratio between the surface-equivalent-sphere diameter, d_A, and the volume-equivalent-sphere diameter, d_{eq}, referred to as flatness, and the circularity, c. The correlation is given by Eq. (17).

$$C_D = \left(\frac{24}{\mathrm{Re}}\frac{d_A}{d_{eq}}\right)\left[1 + \frac{0.15}{\sqrt{c}}\left(\frac{d_A}{d_{eq}}\mathrm{Re}\right)^{0.687}\right] + \frac{0.42\left(\frac{d_A}{d_{eq}}\right)^2}{\sqrt{c}\left[1 + 4.25 \cdot 10^4\left(\frac{d_A}{d_{eq}}\mathrm{Re}\right)^{-1.16}\right]} \tag{16}$$

for the ranges of variables

$0.15 < Re < 1500$,

$0.80 < {}^{d_A}/_{d_{eq}} < 1.50$ and $0.4 < c < 1.0$ [11].

Hölzer & Sommerfeld model

The drag coefficient can also be modeled using the theoretical and experimental correlation for drag in the Stokes region [15], as proposed by Hölzer and Sommerfeld [18]. Their model has its base on the proposal of Leith [15] and Ganser [17] for C_D in the Stokes region, including shape and orientation-dependent terms and the Reynolds number of the particle. The correlation is given by Eq. (18).

$$C_D = \frac{8}{\mathrm{Re}}\frac{1}{\sqrt{\phi_{\parallel}}} + \frac{16}{\mathrm{Re}}\frac{1}{\sqrt{\phi}} + \frac{3}{\sqrt{\mathrm{Re}}}\frac{1}{\phi^{3/4}} + 0.421^{0.4(-\log\phi)^{0.2}}\frac{1}{\phi_{\perp}} \tag{18}$$

where the sphericity, Φ, represents the ratio between the surface area of the volume-equivalent-sphere and that of the particle, the crosswise sphericity, $\phi_{\perp}$, is the ratio between the cross-sectional area of the volume-equivalent-sphere and the projected cross-sectional area of the particle and the lengthwise sphericity, $\phi_{\parallel}$, is the ratio between the cross-sectional area of the volume-equivalent-sphere and the difference between half the surface area and the mean projected longitudinal cross-sectional area of the particle. The correlation is applicable over the entire range of Reynolds numbers up to the critical Reynolds number [18].

Bagheri & Bonadonna model

However, this model is also derived from the Ganser model, which accounts for more accurate and easier shape descriptors rather than sphericity [19]. Here, the form factors, F_S and F_N, are functions of the volume-equivalent-sphere, and three size parameters: the longest, the intermediate, and the shortest lengths of the particle, L, I, and S, respectively. The correlation is given by Eq. (19):

$$C_D = \left(24\frac{k_S}{\mathrm{Re}}\right)\left[1 + 0.125\left(\mathrm{Re}\frac{k_N}{k_S}\right)^{2/3}\right] + \frac{0.46 k_N}{1 + \frac{3305}{\mathrm{Re}\,k_N / k_S}} \tag{19}$$

where the drag corrections, k_N and k_S, are functions of the form factors F_N and F_S.

RESULTS AND DISCUSSION

Grid refinement near the agglomerate walls

To analyze if the turbulence models are applicable, it is important to evaluate the y^+ since the flow near the walls is a relevant region in the study of the drag coefficient. Turbulence models that do not use wall functions need better refinement near walls since their y^+ shall be lower than 1 [40], whereas, in turbulence models that use wall function, the value depends on the type of function treatment. The

Enhanced-Wall functions should be used for values as low as 3 [28]. Since the value of y^+ increases as the velocity of the flow increases, it is necessary to analyze only the highest velocity, i.e., for Reynolds number of 1500.

Simulations presented good results. In general, the y^+ was below 1 for over 99.5% of the elements in the walls of the agglomerates. The RNG k-ε simulations obtained the worst values, where the percentage of elements below 1 varied between 97 and 98%. The values confirm that the meshes are fine enough near the agglomerates and it is reasonable to use the Enhanced-Wall functions for the RSM and RNG k-ε turbulence models and fine enough to use k-ω-based models and the Spalart-Allmaras model.

However, wall functions are approximations for zones near the walls, leading the RSM and RNG k-ε turbulence models to lower efficiency in representing the flow surrounding the agglomerate and models without wall functions. Also, RSM and RNG k-ε turbulence models are expected to correctly represent the flow far from the agglomerates, like the models without wall functions.

Statistical analysis of results – Comparison between simulations and empirical correlations

In Figure 6, we observe three models that present promising curves where simulations are correlated: the Haider and Levenspiel model, the Bagheri and Bonadonna model, and the Tran-Cong model. However, it is important to statistically confirm which model better fits the results obtained in the simulation. The criterion used was the method known as the root-mean-square error (RMSE), calculated by Eq. (3), and which values are presented in Table 4.

Table 4. Root-mean-square error of the turbulence models compared to drag coefficient models.

Agglomerate	Drag coefficient model	Turbulence model				
		RSM	RNG k-ε	SST k-ω	Langtry-Menter	Spalart-Allmaras
3 spheres	Haider & Levenspiel	1.8179	1.5133	1.5568	1.5393	1.2398
	Ganser	2.6035	2.3056	2.3283	2.3185	2.0013
	Tran-Cong *et al.*	2.4351	2.1501	2.1497	2.1484	1.8192
	Hölzer & Sommerfeld	2.3887	2.0893	2.1123	2.1031	1.7805
	Bagheri & Bonadonna	2.4090	2.1157	2.1537	2.1377	1.8560
4 spheres	Haider & Levenspiel	0.7242	0.6639	0.7703	0.9211	0.7223
	Ganser	1.0941	1.0637	1.1173	1.3804	1.0384
	Tran-Cong *et al.*	0.3172	0.3377	0.3112	0.2489	0.3697
	Hölzer & Sommerfeld	0.8041	0.7835	0.8214	1.1276	0.7378
	Bagheri & Bonadonna	0.5447	0.5376	0.5565	0.3474	0.6151
5 spheres	Haider & Levenspiel	1.6936	1.6389	1.7408	1.7140	1.5265
	Ganser	2.4442	2.3938	2.4838	2.4670	2.2444
	Tran-Cong *et al.*	1.0611	1.0464	1.0803	1.0777	0.8359
	Hölzer & Sommerfeld	1.9699	1.9435	1.9937	1.9836	1.7369
	Bagheri & Bonadonna	1.0511	0.9939	1.1009	1.0805	0.9061

Here, we observe that, in most cases, the Tran-Cong model presents lower RMSE for the agglomerates of four and five spheres. An exception is observed for the agglomerate of three spheres, where the Haider and Levenspiel model presented the lower RMSE for all turbulence models tested.

Still analyzing Figure 6, lower deviations of the Haider and Levenspiel model for Reynolds numbers between 1 and 100 were observed. The drag coefficient presents higher values for this range, which interferes the most in the RMSE, compared to the drag values for Reynolds above 100. This behavior generates the distortion that leads to statistical inferring that the Haider and Levenspiel model can better represent the drag coefficient in the agglomerate of 3 spheres. Now, considering the range between 1 and 1500, the plot shows that the Tran-Cong model presents the best agreement with simulation data, while the Haider and Levenspiel present good agreement only for lower Reynolds numbers.

Analysis of the turbulence models

To understand the influence of the turbulence models on the drag coefficient prediction, we first observed the behavior of the streamlines of the flow

surrounding the agglomerate to determine which one better represents three relevant regions of the flow: the boundary layer, the flow far from the walls of the particle and the wake region in the rear of the agglomerates. To infer if the simulation results are consistent, we compared with the literature correlations to observe if simulations follow a trend. At last, we compared the results of the turbulence models with the correlation that better represented the trend of the simulations to find which turbulence model presents lower deviations from the predicted by the correlation.

Before analyzing the drag results, it is relevant to observe if the flow profile corresponds to the expectations from the literature. Militzer *et al.* [46] stated that a particle's aspect ratio substantially interferes with where the separation begins, and the size of the recirculation wake. According to them, particles with similar aspect ratios present similar flow profiles. The flow profile past a sphere is well-known, and since the particle agglomerates are composed of spheres, the flow profile is expected to behave similarly [47]. To compare the velocity profiles, we chose the inlet velocity to reach Re = 1000, where the flow is turbulent, and the vortex street in the rear of the agglomerate is considered fully turbulent [19,35,47]. Figures 3 to 5 present the velocity streamlines for agglomerates of three, four, and five particles, respectively, according to the turbulence models. Comparing the models with wall functions, due to its anisotropic treatment, the RSM is more capable of representing the velocity in the rear of the particle agglomerates in the wake region than the RNG k-ε. However, both do not represent the profile as well as the turbulence models without wall functions. Such behavior confirms the expectation since they model the boundary layer zone to represent it instead of solving the transport equations around the particle.

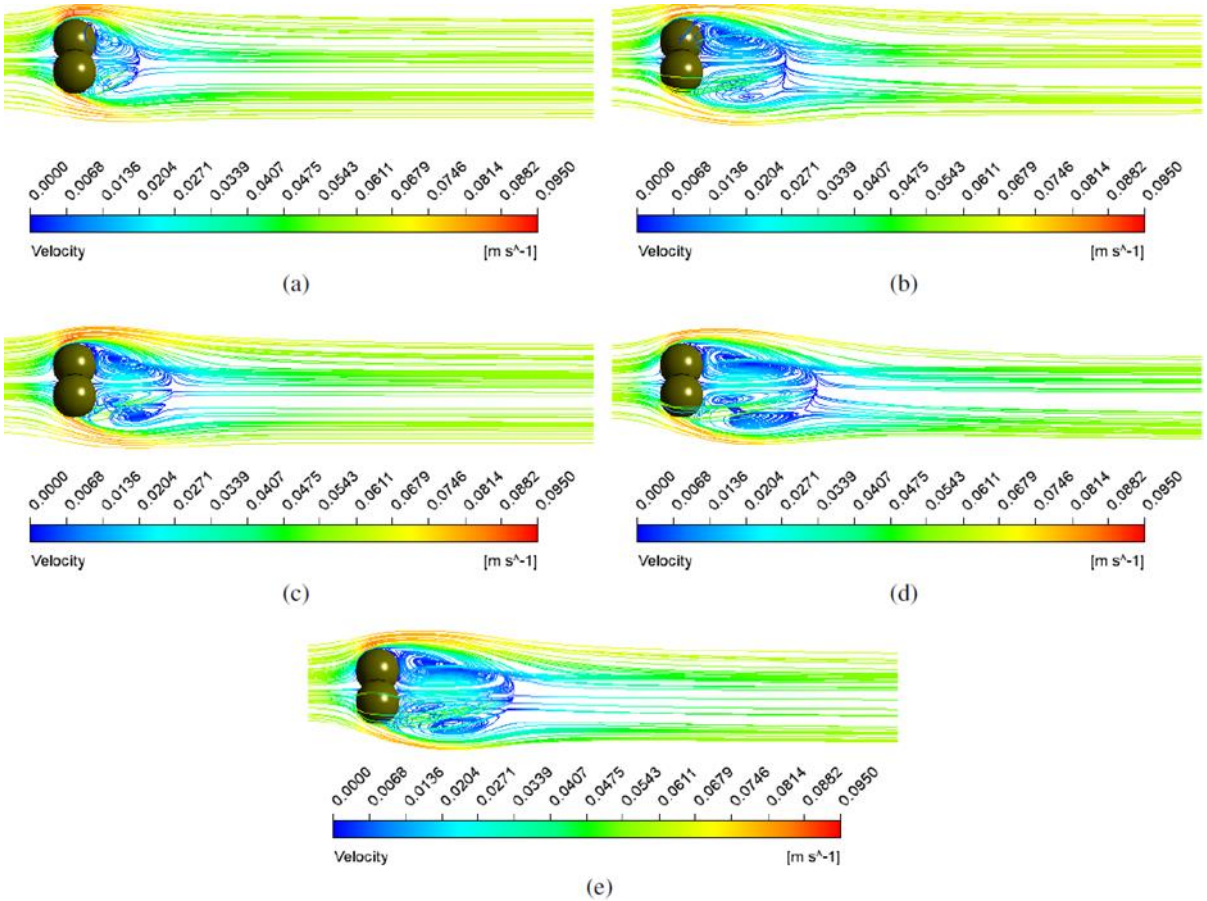

Figure 3. From left to right and top to bottom: velocity streamlines for Re = 1000 in the agglomerate of three particles using the RNG k-ε, RSM, Langtry-Menter, Spalart-Allmaras, and SST k-ω turbulence models.

The velocity streamlines obtained by the SST k-ω model, seen in Figures 3e, 4e, and 5e, better represent the flow profile near the agglomerate walls, i.e., the viscous effects ahead of the particle becoming less important than the inertial effects [19,48]. Such behavior leads to a separation of the flow from the particle at the so-called separation location, and the fluid's inertia is large enough that the fluid cannot follow the path around the rear of the particle. This effect results in a separation bubble after the particle [47] in a region where the boundary layer thickens rapidly in rising pressure, generating a backflow.

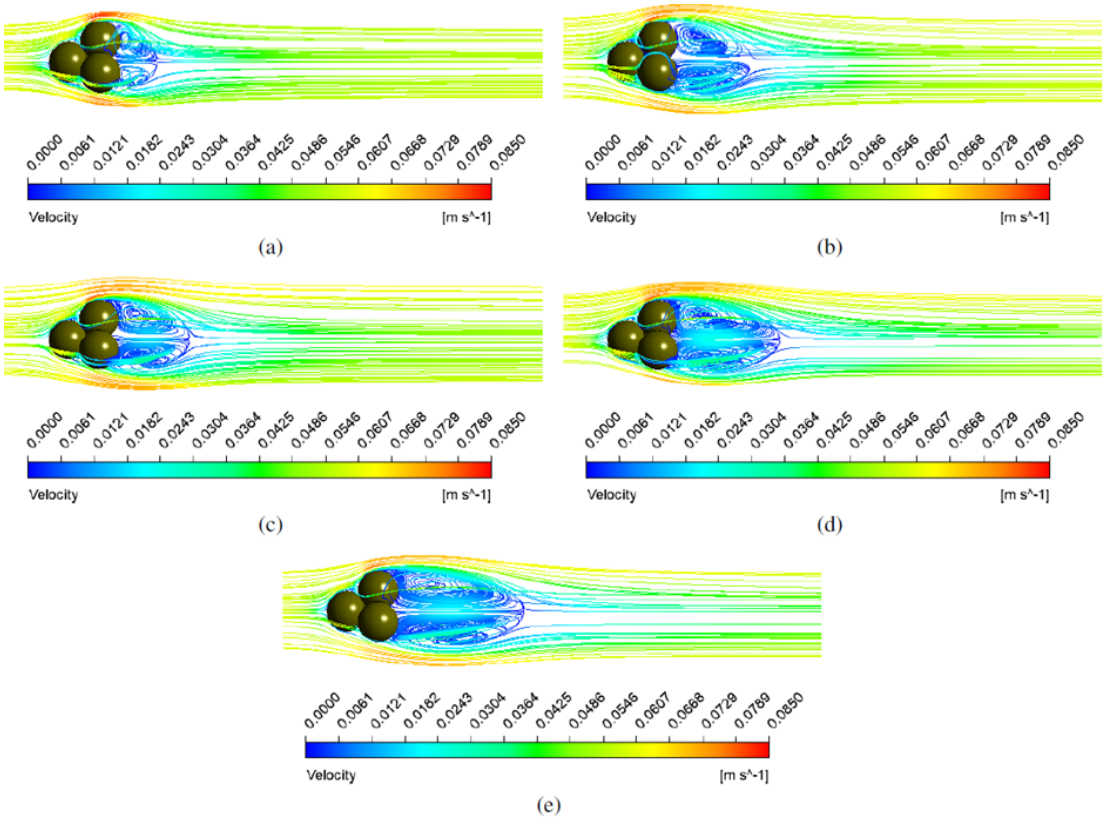

Figure 4. From left to right and top to bottom: velocity streamlines for Re = 1000 in the agglomerate of four particles using the RNG k-ε, RSM, Langtry-Menter, Spalart-Allmaras, and SST k-ω turbulence models..

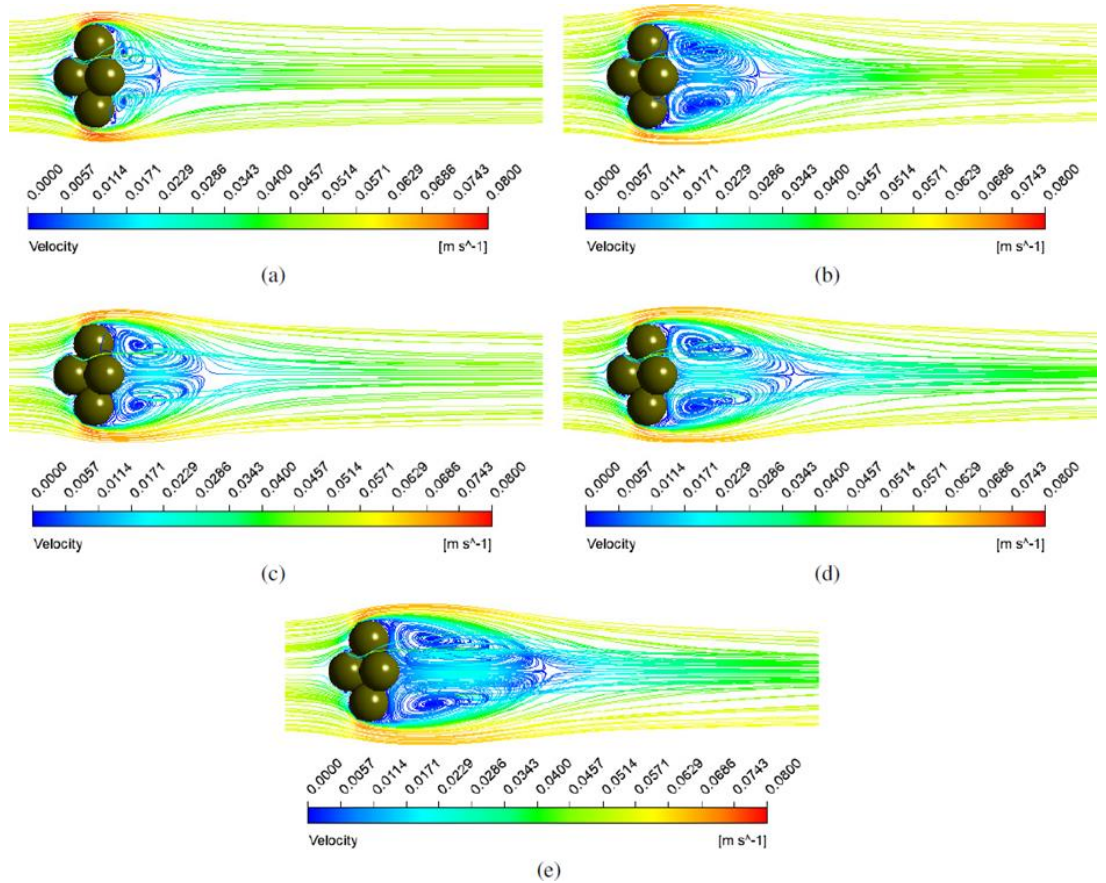

Figure 5. From left to right and top to bottom: velocity streamlines for Re = 1000 in the agglomerate of five particles using the RNG k-ε, RSM, Langtry-Menter, Spalart-Allmaras, and SST k-ω turbulence models.

In the moderate Reynolds number range, e.g., the tested in this study, as the Reynolds number increases, the backflow profile increases in the rear of the particle to regions far from the particle. The SST k-ω model better represented the recirculating profile in the rear of the agglomerates for all the particle agglomerates. However, the separation is unclear for larger Reynolds numbers by order of Re = 105 since it occurs together with the wake region [48]. Consequently, the results of the drag coefficient estimated by simulations using such a model tend to obtain, in general, lower deviations from the empirical model of drag coefficient, as presented in Figure 7.

To find a correlation that better represents the trends of the drag coefficient estimated by simulations, we compared the results of the simulations using the Spalart-Allmaras and the SST k-ω turbulence models with five drag coefficient correlations present in the literature [11,16–19]. The comparisons are presented in Figure 6.

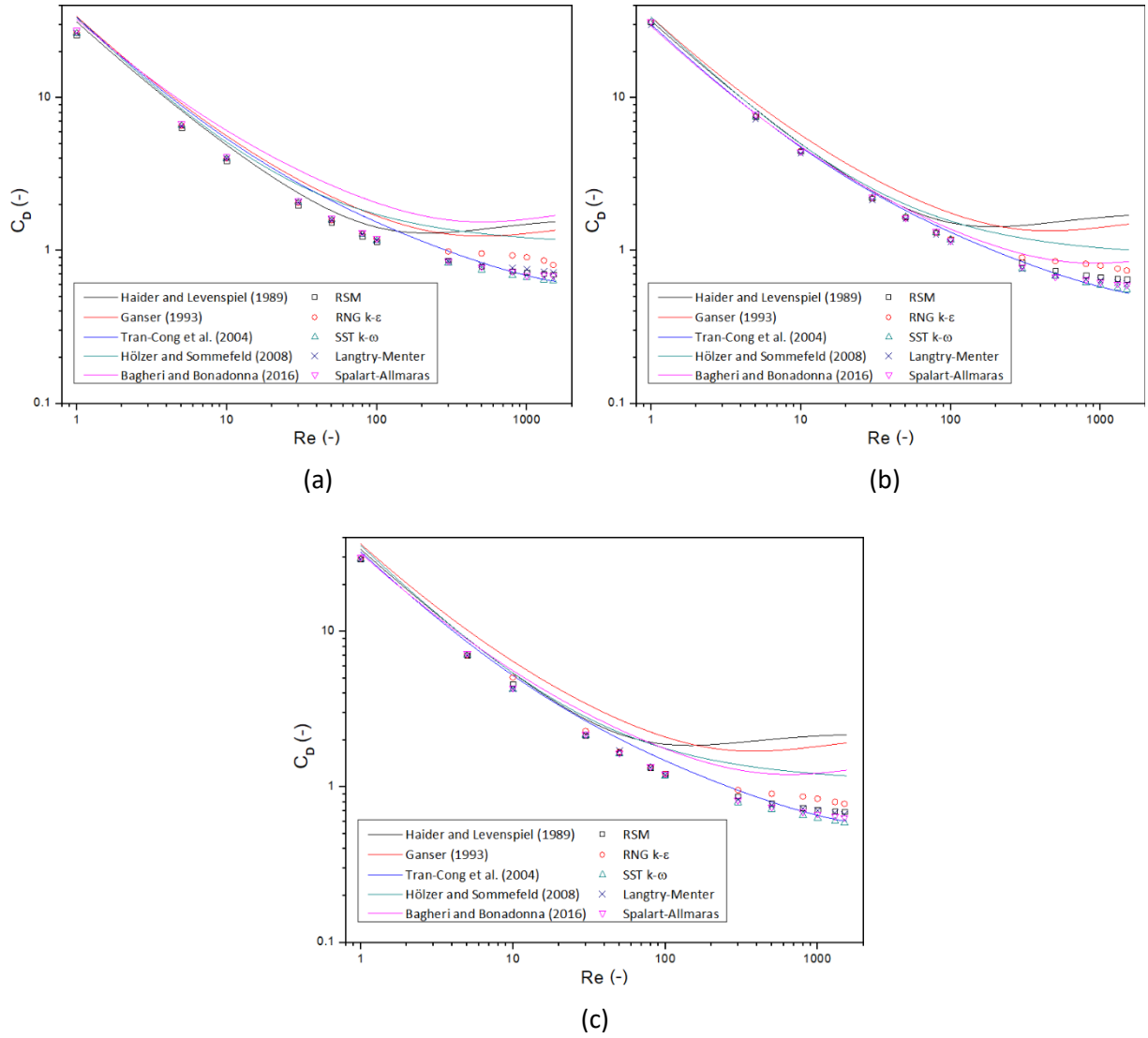

Figure 6. Comparison between predictions of the experimental drag models tested and the simulations data using different turbulence models for agglomerates: a) three particles, b) four particles, and c) five particles.

In a first analysis, one can infer that the simulations correlate better to the Tran-Cong *et al.* [11] model for the three agglomerates along the range of Reynolds numbers tested. An exception occurs in the agglomerate of three particles, as seen in Figure 6a, where the Haider and Levenspiel [16] model has a slightly better representation for Reynolds numbers lower than 10 and a significantly better representation for Reynolds numbers between 10 and 100. Since the range of Reynolds numbers is wide, the logarithm scale

distorts the perception of the deviations.

To reduce the distortion, the relative deviations along the Reynolds number were plotted for the Tran-Cong *et al.* [11] model to analyze if the model represents the simulations and find the turbulence model that presents lower deviations from the correlation. Analyzing the plot of the deviations for the agglomerate of three particles (Figure 7a), the range from 1 to 100 is not so distant from the error of 12% observed in the literature [11]. Also, considering the wide range of Reynolds numbers to which the models are applicable, deviations between ±25% are considered low.

For lower velocities, the flow still follows the curvature of the particle and, consequently, the path around the rear of the particle, for all turbulence models, presented a similar flow profile, leading to similar values for the drag coefficient. As the velocity increases, the edge of the boundary layer gets far from the particle; the boundary layer separation location gets far from the stagnation point, and the turbulence models that use wall functions present difficulties in representing the backflow and wake regions after the particles. Consequently, the RNG k-ε and RSM do not follow the trends observed by the other three turbulence models. The RSM is closer to the trends observed due to its robustness, compared to the RNG k-ε, but in Figures 3 to 5 we observe that the RSM also does not represent so well the velocity profile expected.

Figure 7 shows the deviation of the drag coefficient obtained by simulations compared to the correlation of Tran-Cong *et al.* [11] for the agglomerates in the applicable range of the Reynolds number of the model. The figure shows a trend for all agglomerates, where the deviation slightly and negatively increases as the Reynolds number increases in the range of low Reynolds numbers, from 1 to 100, and for the moderate Reynolds numbers range, from 100 to 1500, the deviation slope is positive and higher.

For Reynolds numbers between 1 and 100, turbulence models presented similar deviations for each of the three agglomerates studied since it corresponds to the laminar regime presenting unseparated flow. The variation between the models results from the different values of the closure constants present in each turbulence model. The deviations begin to diverge for Re ≥ 300, where the flow is transitioning to the turbulence region, and the vortices are becoming present. Figure 7 shows that the values obtained are lower than the predicted by equations, by the magnitude of -25%, -10%, and -18% for the agglomerates of three, four, and five particles, respectively.

As the velocity increases, the gradient of the deviations is positive. However, the slope of the curves for Spalart-Allmaras and SST k-ω models are smoother, and for Reynolds numbers above 1000, the deviations for the SST k-ω present a trend to converge to a value between ± 5%, according to the agglomerate studied. The increase of kinetic turbulence explains so turbulence models that better capture effects in the boundary and outer layers can better estimate the drag force acting in the agglomerate. The streamlines presented in Figures 3 to 5 show that the SST k-ω better represents these effects, followed by the Spalart-Allmaras model, confirming the ability of this model to estimate the drag coefficient in particle agglomerates.

For Reynolds numbers between 10 and 100, the deviations are constant or close to constant – in the case of the agglomerate of four particles. It corresponds to the range where the von Kármán vortex street starts to appear in a laminar flow, depending on the body's shape and the fluid's kinematic viscosity. The deviations varied from -13 to -28% in the agglomerate of three particles, -6 to -14% in the agglomerate of four particles, and -13 to -20% in the agglomerate of five particles. However, simulations with Reynolds numbers below 10 have drag coefficients closer to the estimated correlation.

The symmetry of the agglomerate is an important variable to consider in the analysis. In numerical simulations, symmetric geometries are easier to generate meshes with good refinement quality in the boundary layer separation region. It leads to better results and reduces errors of pressure and velocity fields, mainly near walls, where the drag and lift are computed. The capacity to predict the flow profile and the adverse pressure gradient is correlated with the geometry since the interference of the effect between the spheres of each agglomerate of particles is reduced as the symmetry of the agglomerate increases. Physically, it means that symmetric geometries tend to generate symmetric streamlines, which are easier to be calculated by turbulence models. Such behavior is well presented in Figure 7, where the agglomerate of four particles has lower deviations since its symmetry is closer to a single sphere – the most symmetrical shape for spheric particle agglomerates – followed by the agglomerate of five and three particles.

Still analyzing the geometry of the agglomerates, it is possible to see that they generate curvature in the streamlines as we increase the velocity, which directly affects the turbulence and, consequently, the flow profile. The curvature effect can highly decrease the Reynolds stress normal to the wall as the ratio between the boundary layer thickness and the radius increases. Such a decrease reaches up to 50% for a ratio of 0.03 [49].

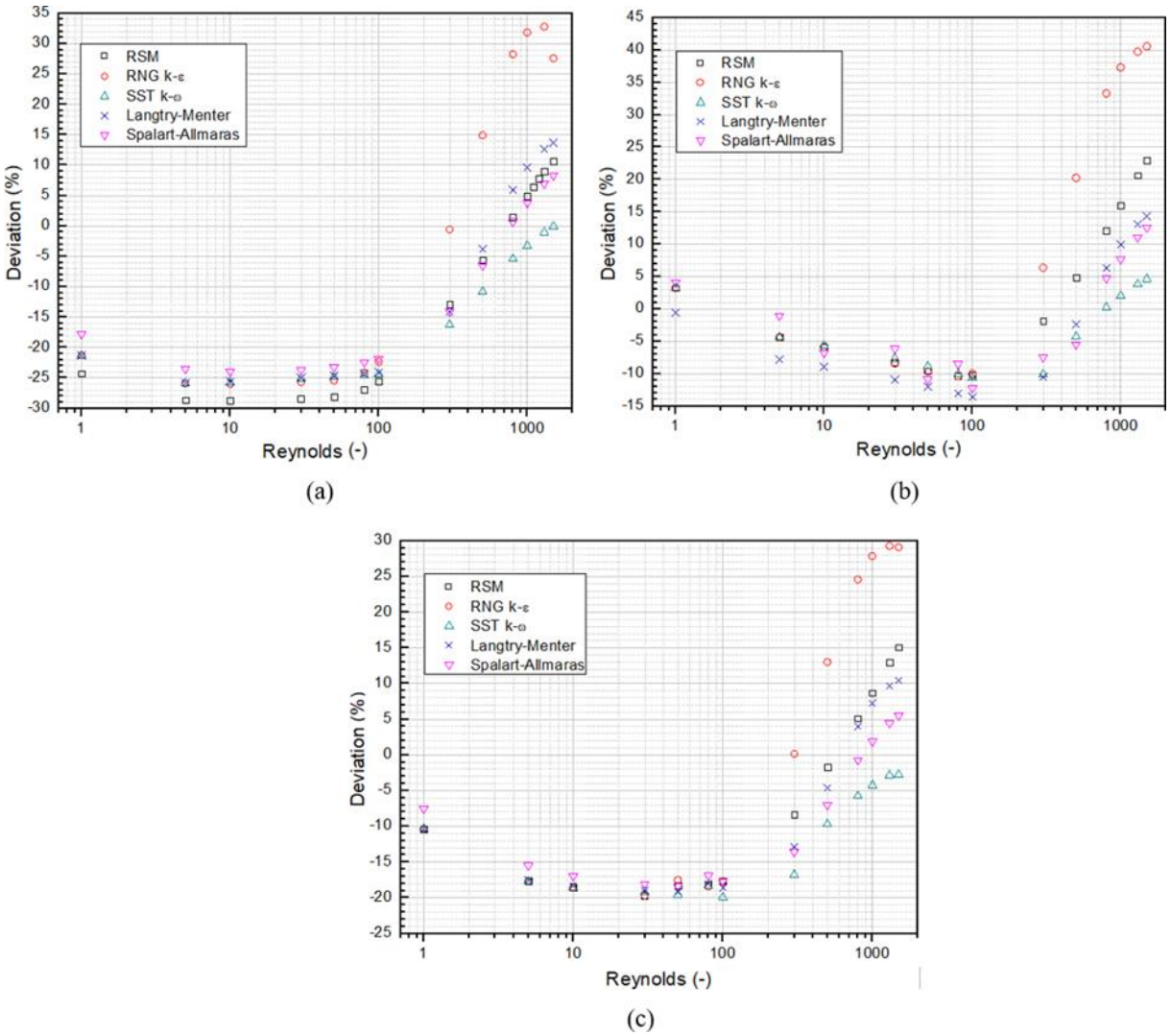

Figure 7. From left to right and top to bottom: deviations of simulated data from the Tran-Cong model for the agglomerate of three, four, and five particles.

The simulations confirmed the expectations of better results when the curvature effects are considered using the Spalart-Allmaras and both SST k-ω-based models [50].

Since the geometry in the agglomerate of four particles is closer to a single sphere, the deviations are lower for the turbulence models that do not use wall functions. Turbulence models such as the RSM and RNG k-ε are accurate in computing the field far from the agglomerate; however, the near-wall regions and boundary layers are not correctly presented, with difficulties in representing the adverse pressure gradient of the agglomerate in a greater area, lacking the quality to compute the drag coefficient, increasing the deviation. It is related to the fact that the wall-functions effects are more influential in the turbulence model than the curvature effects present in a sphere, so the pressure and velocity fields are not well represented near the walls as in the other turbulence models.

The results of this study demonstrate that the utilization of the steady formulation approach yields accurate estimations of the drag coefficient. Furthermore, the turbulence model plays a crucial role in effectively modeling the problem, not only for estimating the drag coefficient but also for accurately predicting the flow profile in regions characterized by separation and recirculating wakes, particularly in flows with higher Reynolds numbers. The implementation of RANS turbulence models that calculate the flow field near the particles instead of relying on wall-function modeling exhibited robustness in representing the presented problem. Moreover, these models agreed more closely with experimental correlations for drag estimation in particle agglomerates.

The simplifications proposed in this study offer a significant advantage, primarily through the reduction of computational time required to obtain results. Consequently, this reduction allows for more simulations to be conducted, facilitating a more detailed

presentation of the drag coefficient curve and enabling the proposal of new correlations. By incorporating these findings into future research, it is possible to advance the understanding of drag coefficient estimation and develop improved correlations for industrial-scale problems.

CONCLUSION

The present study carried out steady simulations of three irregularly-shaped particle agglomerates composed of spherical particles surrounded by water. The drag coefficient at different inlet conditions was obtained for five different turbulence models and compared with five correlations in the literature to predict the drag coefficient in agglomerates to understand which numerical setup better represents the flow. The proposed methodology presented a good agreement with experimental correlations of drag coefficient estimation, which is useful for reducing the time and computational efforts required to numerically obtain the drag acting in particle agglomerates and robustness to estimate the drag coefficient in higher Reynolds numbers. The main observations were:

Steady RANS turbulence models showed good agreement with the literature to estimate the drag coefficient on particle agglomerates, without the drawback of high computational cost seen in unsteady simulations, such as URANS, LES, DNS, or LBM.

The turbulence closure equations present a lower influence in the evaluation of flow fields for $1 \leq Re \leq 100$, so the drag coefficients estimated for each turbulence model are very similar.

The flow profile is better represented using turbulence models with no wall functions. Spalart-Allmaras and SST k-ω models could represent the flow near the particle agglomerates and far from its walls; however, the second one was more robust.

Steady formulation with the SST k-ω turbulence model can represent the flow for a wide range of Reynolds numbers with less computational effort.

Despite presenting the best agreement with Tran-Cong *et al.*[11] model, the numerical results presented relative deviations by a magnitude of -20%, mainly for lower Reynolds numbers, representing a good agreement since the average error of the empirical correlation is 10%.

Reduced computational costs make it possible to obtain more data so that further studies can focus on elaborating new accurate correlations to be scaled up for industry-scale problems.

The proposed numerical methodology was useful for initial tests and experimental validation.

NOMENCLATURE

A, B, C, D	Parameters of the Haider and Levenspiel drag model
A_P	Projected area
C	Circularity
C_D	Drag coefficient
$CDcorr$	Drag coefficient estimated by correlations
$CDsim$	Drag coefficient estimated by simulations
d_A	Surface-equivalent-sphere diameter
d_{eq}	Volume-equivalent-sphere diameter
F_D	Drag force
K	Fluctuation kinetic energy
K	Turbulence kinetic energy
k_N	Newton's parameter
k_S	Stokes' parameter
N	Total data in the sample studied
P_k	Production of turbulent kinetic energy
Re	Reynolds number
$Re\theta t$	Transition momentum thickness Reynolds number
T	Time
u_f	Fluid velocity
u_p	Particle velocity
xi	Value of the i^{th} data estimated by correlations
x_i	Value of the i^{th} data obtained by simulation
γ	Intermittency
δ	Percent deviation
ε	Turbulence dissipation rate
ν	Kinematic viscosity
ν_t	Turbulent kinematic viscosity
$\tilde{\nu}$	Spalart-Allmaras kinematic viscosity
ρ	Density
τ_{ij}	Specific Reynolds stress tensor
ϕ	Sphericity
$\phi_\perp$	Crosswise sphericity
$\phi_\parallel$	Lengthwise sphericity
ω	Specific turbulence dissipation

ACKNOWLEDGMENTS

This study was partly financed by the Coordination for the Improvement of Higher Education Personnel (CAPES) - Finance Code 001. The authors would like to thank also the National Council for Scientific and Technological Development (CNPq, grant number 140412/2020-4) for the financial support of this work.

REFERENCES

[1] J. Wang, W. Ge, J. Li, Chem. Eng. Sci. 63 (2008) 1553–1571. https://doi.org/10.1016/j.ces.2007.11.023.

[2] E.U. Hartge, L. Ratschow, R. Wischnewski, J. Werther, Particuology 7 (2009) 283–296.

https://doi.org/10.1016/j.partic.2009.04.005.

[3] A. Nikolopoulos, D. Papafotiou, N. Nikolopoulos, P. Grammelis, E. Kakaras, Chem. Eng. Sci. 65 (2010) 4080–4088. https://doi.org/10.1016/j.ces.2010.03.054.

[4] L. Wang, C. Wu, W. Ge, Powder Technol. 319 (2017) 221–227. https://doi.org/10.1016/j.powtec.2017.06.046.

[5] D. Gidaspow, in Multiphase Flow and Fluidization: Continuum and Kinetic Theory Descriptions with Applications, Academic Press, Cambridge (1994). ISBN: 978-0-122-82470-8.

[6] R.J. Hill, D.L. Koch, A.J.C. Ladd, J. Fluid Mech. 448 (2001) 213–241. https://doi.org/10.1017/S0022112001005948.

[7] R.J. Hill, D.L. Koch, A.J.C. Ladd, J. Fluid Mech. 448 (2001) 243–278. https://doi.org/10.1017/S0022112001005936.

[8] M.A. van der Hoef, R. Beetstra, J.A.M. Kuipers, J. Fluid Mech. 528 (2005) 233–254. https://doi.org/10.1017/S0022112004003295.

[9] R.C. Senior, C. Brereton, Chem. Eng. Sci. 47 (1992) 281–296. https://doi.org/10.1016/0009-2509(92)80020-D.

[10] K. Kuwagi, K. Takano, M. Horio, Powder Technol. 113 (2000) 287–298. https://doi.org/10.1016/S0032-5910(00)00311-9.

[11] S. Tran-Cong, M. Gay, E.E. Michaelides, Powder Technol. 139 (2004) 21–32. https://doi.org/10.1016/j.powtec.2003.10.002.

[12] D.A. Deglon, C.J. Meyer, Miner. Eng. 19 (2006) 1059–1068. https://doi.org/10.1016/j.mineng.2006.04.001.

[13] G.L. Lane, Chem. Eng. Sci. 169 (2017) 188–211. https://doi.org/10.1016/j.ces.2017.03.061.

[14] R. Clift, J.R. Grace, M.E. Weber, Bubbles, Drops and Particles, Academic Press, Cambridge (1978). ISBN: 978-0-121-76950-5.

[15] D. Leith, Aerosol Sci. Technol. 6 (1987) 153–161. https://doi.org/10.1080/02786828708959128.

[16] A. Haider, O. Levenspiel, Powder Technol. 58 (1989) 63–70. https://doi.org/10.1016/0032-5910(89)80008-7.

[17] G.H. Ganser, Powder Technol. 77 (1993) 143–152. https://doi.org/10.1016/0032-5910(93)80051-B.

[18] A. Hölzer, M. Sommerfeld, Powder Technol. 184 (2008) 361–365. https://doi.org/10.1016/j.powtec.2007.08.021.

[19] G. Bagheri, C. Bonadonna, Powder Technol. 301 (2016) 526–544. https://doi.org/10.1016/j.powtec.2016.06.015.

[20] R. Beetstra, M. van der Hoef, J. Kuipers, Comput. Fluids 35 (2006) 966–970. https://doi.org/10.1016/j.compfluid.2005.03.009.

[21] N.G. Deen, S.H.L. Kriebitzsch, M.A. van der Hoef, J.A.M. Kuipers, Chem. Eng. Sci. 81 (2012) 329–344. https://doi.org/10.1016/j.ces.2012.06.055.

[22] S.B. Pope, Turbulent Flows, Cambridge University Press, Cambridge, (2000). ISBN: 978-0-521-59886-6.

[23] S. Heinz, Prog. Aerosp. Sci. 114 (2020) 100597. https://doi.org/10.1016/j.paerosci.2019.100597.

[24] S.Y. Chen, G.D. Doolen, Annu. Rev. Fluid Mech. 30 (1998) 329–364. https://doi.org/10.1146/annurev.fluid.30.1.329.

[25] M. Dietzel, M. Sommerfeld, Powder Technol. 250 (2013) 122–137. https://doi.org/10.1016/j.powtec.2013.09.023.

[26] M. Mehrabadi, E. Murphy, S. Subramaniam, Chem. Eng. Sci. 152 (2016) 199–212. https://doi.org/10.1016/j.ces.2016.06.006.

[27] S. Chen, P. Chen, J. Fu, Phys. Fluids 34 (2022) 023307. https://doi.org/10.1063/5.0082653.

[28] ANSYS, Inc, ANSYS Fluent 14.5 Theory Guide (2012). http://www.pmt.usp.br/academic/martoran/notasmodelosgrad/ANSYS%20Fluent%20Theory%20Guide%2015.pdf [accessed 15 February 2023].

[29] J. Ferziger, M. Perić, R.L. Street, Computational Methods for Fluid Dynamics, Springer, New York, (2002). ISBN: 978-3-319-99693-6.

[30] P.R. Spalart, S.R. Allmaras, Technical Report AIAA-92-0439 1 (1992) 5–21. https://doi.org/10.2514/6.1992-439.

[31] V. Yakhot, S.A. Orszag, S. Thangam, T.B. Gatski, C.G. Speziale, Phys. Fluids A 7 (1992) 1510–1520. https://doi.org/10.1063/1.858424.

[32] F.R. Menter, AIAA J. 32 (1994) 1598–1605. https://doi.org/10.2514/3.12149.

[33] R.B. Langtry, F.R. Menter, AIAA J. 47 (2009) 2894–2906. https://doi.org/10.2514/1.42362.

[34] B.E. Launder, G.J. Reece, W. Rodi, J. Fluid Mech. 68 (1975) 537–566. https://doi.org/10.1017/S0022112075001814.

[35] W.R.A. Goossens, Powder Technol. 352 (2019) 350–359. https://doi.org/10.1016/j.powtec.2019.04.075.

[36] E. Loth, Powder Technol. 182 (2008) 342–353. https://doi.org/10.1016/j.powtec.2007.06.001.

[37] J.P. van Doormaal, G.D. Raithby, Numer. Heat Transfer 7 (1984) 147–163. https://doi.org/10.1080/01495728408961817.

[38] H.K. Versteeg, W. Malalasekera, An Introduction to Computational Fluid Dynamics: The Finite Volume Method, Pearson Education Limited, Harlow, (2007). ISBN: 978-0-131-27498-3.

[39] Z. Tuković, M. Perić, H. Jasak, Comput. Fluids 166 (2018) 78–85. https://doi.org/10.1016/j.compfluid.2018.01.041.

[40] D.C. Wilcox, Turbulence Modeling for CFD, DCW Industries, La Cañada, (2004). ISBN: 978-1-928729-08-2.

[41] B.E. Launder, B.I. Sharma, Lett. Heat Mass Trans. 1 (1974) 131–138. https://doi.org/10.1016/0094-4548(74)90150-7.

[42] J.L. Isaacs, G. Thodos, Can. J. Chem. Eng. 45 (1967) 150–155. https://doi.org/10.1002/cjce.5450450306.

[43] R. Clift, W.H. Gauvin, Can. J. Chem. Eng. 49 (1971) 439–448. https://doi.org/10.1002/cjce.5450490403.

[44] E.K. Marchildon, W.H. Gauvin, AIChE J. 25 (1979) 938–948. https://doi.org/10.1002/aic.690250604.

[45] R.P. Chhabra, L. Agarwal, N.K. Sinha, Powder Technol. 101 (1999) 288–295. https://doi.org/10.1016/S0032-5910(98)00178-8.

[46] J. Militzer, J. M. Kan, F. Hamdullahpur, P.R. Amyotte, A.M. Al Taweel, Powder Technol. 57 (1989) 193–195. https://doi.org/10.1016/0032-5910(89)80075-0.

[47] R. Ouchene, Phys. Fluids 32 (2020) 073303. https://doi.org/10.1063/5.0011618.

[48] B.R. Munson, D.F. Young, T.H. Okiishi, Fundamentals of Fluid Mechanics, John Wiley & Sons, Hoboken, (2016). ISBN: 978-1-119-54799-0.

[49] B.E. Thompson, J.H. Whitelaw, J. Fluid Mech. 157 (1985) 305–326. https://doi.org/10.1017/S0022112085002397.

[50] L. Davidson, J. Fluids Eng. 117 (1995) 50–57. https://doi.org/10.1115/1.2816818.

RICARDO ARBACH FERNANDES DE OLIVEIRA

JULIO HENRIQUE ZANATA

GABRIELA CANTARELLI LOPES

Department of Chemical Engineering, Federal University of São Carlos, São Carlos - São Paulo - Brazil

NUMERIČKO ISTRAŽIVANJE TURBULENCIJE ODREĐIVANJEM KOEFICIJENTA OTPORA ZA AGLOMERATE ČESTICA

Numeričke simulacije strujanja oko aglomerata čestica su sprovedene korišćenjem računarske dinamike fluida da bi se ocenila sposobnost pet modela turbulencije RANS da procene koeficijent otpora za aglomerate čestica. Simulacije su sprovedene u stacionarnim uslovima za Rejnoldsove brojeve između 1 i 1500. Strujnice su pokazale da simetrični aglomerati imaju profil brzine sličan profilu jedne sfere. Rezultati su pokazali da i Spalart-Allmaras i SST k-ω modeli turbulencije mogu predstaviti profil protoka u regionima blizu i daleko od zidova aglomerata i mrtve zone iza aglomerata. RNG k-ε model loše predviđa profil brzine i koeficijent otpora. Koeficijent otpora se bolje predstavlja modelom Tran-Kong, koji pokazuje da su se odstupanja od predviđanja koeficijenta otpora za aglomeratima česticasmanjivala kako se povećava gustina pakovanja aglomerata. Upotreba stabilnih RANS simulacija je izvodljiva i efikasna metoda predviđanja, uz niske računarske troškove. Za prelazne i turbulentne režime strujanja, rezultati su pokazali dobru saglasnost, sa odstupanjima između -15% i 13%, dok su za niže Rejnoldsove brojeve odstupanja varirala između -25% i 5%.

Ključne reči: čvrste materije, aglomerati čestica, turbulencija, koeficijent otpora, računarska dinamika fluida.

NAUČNI RAD